

See discussions, stats, and author profiles for this publication at: <https://www.researchgate.net/publication/340627594>

# Fusion of deep-learned and hand-crafted features for cancelable recognition systems

Article in Soft Computing · April 2020

DOI: 10.1007/s00500-020-04856-1 |

---

CITATIONS  
6

READS  
484

---

12 authors, including:



Essam Abdellatef

Faculty of engineering; Sinai University; Egypt

21 PUBLICATIONS 235 CITATIONS

[SEE PROFILE](#)



Eman M Omran

Menoufia University

6 PUBLICATIONS 51 CITATIONS

[SEE PROFILE](#)

Randa Soliman

Menoufia University

17 PUBLICATIONS 246 CITATIONS

[SEE PROFILE](#)



Nabil A. Ismail

Faculty of Electronic Engineering Menoufia University

209 PUBLICATIONS 767 CITATIONS

[SEE PROFILE](#)



# Fusion of deep-learned and hand-crafted features for cancelable recognition systems

Essam Abdellatef<sup>1</sup> · Eman M. Omran<sup>2</sup> · Randa F. Soliman<sup>3</sup> · Nabil A. Ismail<sup>4</sup> · Salah Eldin S. E. Abd Elrahman<sup>4</sup> · Khalid N. Ismail<sup>5,6</sup> · Mohamed Rihan<sup>7</sup> · Fathi E. Abd El-Samie<sup>7,8</sup> · Ayman A. Eisa<sup>2</sup>

© Springer-Verlag GmbH Germany, part of Springer Nature 2020

## Abstract

The recent years have witnessed a dramatic shift in the way of biometric identification, authentication, and security processes. Among the essential challenges that face these processes are the online verification and authentication. These challenges lie in the complexity of such processes, the necessity of the personal real-time identifiable information, and the methodology to capture temporal information. In this paper, we present an integrated biometric recognition method to jointly recognize *face, iris, palm print, fingerprint and ear* biometrics. The proposed method is based on the integration of the extracted deep-learned features together with the hand-crafted ones by using a fusion network. Also, we propose a novel convolutional neural network (CNN)-based model for deep feature extraction. In addition, several techniques are exploited to extract the hand-crafted features such as histogram of oriented gradients (HOG), oriented rotated brief (ORB), local binary patterns (LBPs), scale-invariant feature transform (SIFT), and speeded-up robust features (SURF). Furthermore, for dimensional consistency between the combined features, the dimensions of the hand-crafted features are reduced using independent component analysis (ICA) or principal component analysis (PCA). The core of this paper is the template protection via a cancelable biometric scheme without significantly affecting the recognition performance. Specifically, we have used the bio-convolving approach to enhance the user's privacy and ensure the robustness against spoof attacks. Additionally, various CNN hyper-parameters with their impact on the proposed model performance are studied. Our experiments on various datasets revealed that the proposed method achieves 96.69%, 95.59%, 97.34%, 96.11% and 99.22% recognition accuracies for face, iris, fingerprint, palm print and ear recognition, respectively.

**Keywords** Deep learning · Feature fusion · Cancelable biometrics

## 1 Introduction

Biometrics achieve a promising performance for the personal verification and authentication in many applications, which include law enforcement, forensics, immigration, border, and access control. Unlike passwords or tokens that

---

Communicated by V. Loia.

---

✉ Essam Abdellatef  
essam\_abdellatef@yahoo.com

Eman M. Omran  
omran\_eman91@yahoo.com

Randa F. Soliman  
randafouad2010@yahoo.com

Nabil A. Ismail  
nabil.Ismail@el-eng.menofia.edu.eg

Salah Eldin S. E. Abd Elrahman  
salaheldeen@el-eng.menofia.edu.eg

Khalid N. Ismail  
khalid.n.ismail@gmail.com

Mohamed Rihan  
mohamed.elmelegy@el-eng.menofia.edu.eg

Fathi E. Abd El-Samie  
fathi\_sayed@yahoo.com

Ayman A. Eisa  
Ayman\_Eisa@yahoo.com

Extended author information available on the last page of the article

could be forgotten, stolen or lost, the biometric recognition systems (Jain 2004, 2006) do not suffer from such problems and may achieve a better security performance. The biometric attributes are categorized into *stable* and/or *behavioral* characteristics. The *stable* characteristics contain *face*, *iris*, *fingerprint*, *palm print*, and *ear shape*. The behavioral traits deal with the *behavioral* characteristics like the *key stroke pattern* and *signature*.

Recently, trends targeted the automation of biometric identification, while maintaining the authentication security. Since CNNs represent one of the key mechanisms for resolving computer vision issues, the CNN-based systems can perform all recognition methods. Therefore, the robustness and distinctive characteristics introduced by CNNs have been utilized for biometric recognition, image classification, and object detection. Face recognition (FR) is commonly used for individuals' recognition. It is based on some spatial metrics like size, shape and face structure of a person. A human face is considered as one of the most effective biometric traits compared to other biometrics due to the low cost, contactless nature, and high acceptability during acquisition (Pichao et al. 2016; Tomas et al. 2016; Xiaolin and Yicong 2018; Mariana-Iuliana et al. 2019).

The automation of the individuals' recognition is based on their iris traits in a framework called *iris recognition* (IR). Moreover, the IR techniques revealed high matching rates with large datasets. This distinctive success is attributed to the sophisticated iris stroma texture which differs upon persons, the permanent perception of iris special features, and the genetic limitation penetration of the iris (Daugman 2016). Superior recognition rates of the applicable techniques for IR have been achieved by the National Institute of Science and Technology (NIST) (2012).

*Fingerprint recognition* is used as a biometric solution for authentication on computerized systems due to the ease of fingerprint acquisition. In addition, for everyone, there are ten sources of biometrics. In fingerprint recognition systems, a person may be recognized using the features of minutiae points and ridges (Bolle et al. 2002). *Palm print* recognition (Ratha et al. 2007) depends on unique patterns of various characteristics in palms of people's hands for the recognition operation. The *palm print* and *fingerprint* recognition systems include similar details, and hence they are used together to improve the personal identification accuracy. *Ear recognition* (Omara et al. 2016) could be used for personal identification and authentication due to universality, distinctiveness, permanence and collectability of ear patterns. Additionally, the structure of an ear does not change radically over time.

Nowadays, the protection of biometric data got more attention. The cancelable biometric recognition techniques could be used for the protection of biometric data

depending on template transformation schemes. This is based on intentional repeated distortions to achieve security for biometric templates. The distortions could be performed either at the feature level or at the image level. Ratha et al. (2006) firstly introduced the notion of biometrics cancelability. They rearranged the fingerprint minutiae in polar and cartesian domains to obtain the cancelable templates. Although their work renders the satisfactory accuracy performance, the non-invertibility was seen weak (Harjoko et al. 2009). Meanwhile, the work presented in Ratha et al. (2006) inspired IrisCode protection schemes later (Ignat et al. 2013). Instead of using the whole iris template as reported in Chin et al. (2006), Pillai et al. (2010) used sectorized random projections for generating the cancelable iris templates. Rathgeb et al. (2010) and Zuo et al. (2008) suggested the generation of the cancelable iris templates by applying the row permutation on IrisCodes. In Tarek et al. (2017), a random key was used to convert an online signature data into discrete sequences that are convolved together to create the cancelable template. A one more cancelable biometric method has been presented by Teoh et al. (2004) for increasing recognition rates of cancelable templates. Rathgeb et al. (2014, 2015) used bloom filters to construct cancelable templates from iris codes.

In this research paper, a cancelable biometric recognition method is proposed. This method incorporates the use of a fusion network to combine deep features (DFs) with hand-crafted features. The DFs are extracted using a CNN and the hand-crafted features are extracted using traditional feature extraction algorithms. The bio-convolving method is applied to provide protection of the biometric data. The main contributions of this work can be listed as follows:

1. Proposal of a CNN model for deep-learned feature extraction. The proposed CNN incorporates a depth concatenation and residual learning block (ReSBL). Also, the proposed model consists of “22” convolutional, “8” max-pooling, “1” batch normalization, “1” fully-connected, “1” feature normalization and “1” softmax layers.
2. Proposal of cancelable *face*, *iris*, *fingerprint*, *palm print* and *ear* recognition systems based on generating a new template from fusing the extracted deep-learned features together with the hand-crafted ones by using a fusion network, and then applying the bio-convolving approach on the fused result to provide a cancelable feature descriptor.
3. Study of the effect of different hand-crafted feature extraction techniques such as SURF, ORB, LBPs, SIFT, and HOG on the recognition performance.
4. For dimensional consistency between the fused features, we perform reduction of the dimensions of the

hand-crafted features. Furthermore, the influence of two different dimensionality reduction techniques, which are ICA and PCA, on the recognition performance, is studied.

## 5 Tuning of different CNN hyper-parameters and study of their impact on the performance.

The remaining parts of this article are organized as follows. Section 2 presents the main ideas that have been manipulated in the literature. Section 3 presents the proposed method. Section 4 illustrates the experimental results, and Sect. 5 gives the concluding remarks of the presented work.

## 2 Related work

Biometric recognition systems, which are widely used for individuals' recognition, have a set of advantages over traditional password/token-based authentication schemes. So, research works aimed to tackle the related issues and sorted out many challenges for biometric recognition systems. The CNNs are used in several computer vision applications such as recognition of objects and image segmentation (LeCun et al. 2015; Bengio et al. 2013). The CNNs belong to a certain deep learning category that aims to processing of videos and images. Moreover, CNNs are capable not only of automating learning of image features, but also of overcoming the disadvantages of a lot of conventional hand-crafted feature extraction schemes (Deng et al. 2017a, b; Zhao et al. 2017, 2018). The earliest DeepFace (Taigman et al. 2014) trained a CNN on nearly 4.4E6 face images, and it adopted a CNN for feature extraction in the face verification tasks. Furthermore, this technique reached an accuracy of 97.35% when applied on Labeled Faces in the Wild (LFW) dataset with 4096-D feature vectors. In extending DeepFace, a semantic bootstrapping has been applied to choose more efficient training sets from the large databases (Taigman et al. 2015). In Sun et al. (2015), the intra-class distance is decreased, and the verification losses are further integrated.

Few deep networks have been introduced for enhancing the iris recognition performance. DeepIris network was presented by Liu et al. (2016). The deep network proposed in Liu et al. (2016) attained a superior recognition rate on various databases. DeepIrisNet-A (Gangwar and Joshi 2016) achieved a superior performance on various databases (Phillips et al. 2010). Zhu et al. (2005) trained the neural network to estimate the correct ridge orientation of the fingerprint. Liu et al. (2010) used the neural networks based on backward propagation for detecting unique points from the gray-scale fingerprint images. Yang et al. (2005) used the neural networks to extract the minutiae points

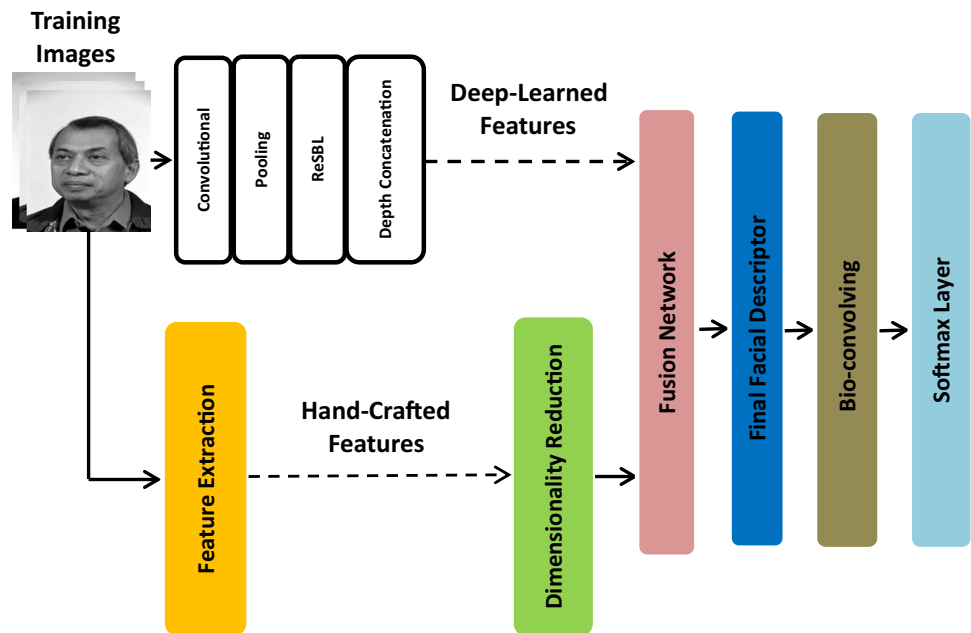
from the gray-scale images. Sarbadhikari et al. (1998) used two-stage classifiers for fingerprint image classification. In Xu et al. (2016), a method has been presented relying on a multi-class projection extreme learning machine (MPELM) dataset to enhance the recognition performance of multi-spectral palm prints. This method achieved an accuracy of 97.33%. In Ekinci and Aykut (2007), a Gabor wavelet-based kernel has been proposed for the palm print recognition, and it realized an accuracy of 95.17%. In Connie et al. (2005), the palm print images were aligned and Fisher discriminant analysis (FDA) was applied. Emersic et al. (2017) adopted the data augmentation approach for the ear recognition to overcome the problem of insufficient labeled data. In addition, the selective learning technique was implemented to decrease the over-fitting problem. SqueezeNet (Iandola et al. 2016) was also evaluated on an unconstrained ear database. In Emersic et al. (2017) and Pedro et al. (2016), computer vision laboratory (CVL) and annotated web ears (AWE) datasets were combined to obtain enough data.

The increasing demand for providing security and privacy of biometric templates raises more challenges for recognition systems. Thanks to cancelable biometric recognition techniques (Polash et al. 2014), biometric data protection could be provided with a slight degradation in the system performance. Cancelable biometric techniques adopt the transformation of the original biometric templates using a one-way function. This strategy provides irreversibility, which means that no information about the original biometric templates could be obtained from the transformed ones.

## 3 The proposed recognition method

For the biometric recognition improvement, we think of performing the recognition operation based on a hybrid feature descriptor. The hand-crafted and DFs are fused together using a fusion network to form a single feature vector for classification. The proposed framework is displayed in Fig. 1. Firstly, the input images are split into training and testing images. The training images are fed to the proposed CNN model to generate the DFs using (deep feature extraction layers such as convolutional, pooling, ReSBL, and depth concatenation layers). Additionally, various techniques are applied on the training images to extract the hand-crafted features. Several traditional methods are examined, such as HOG (Ali et al. 2017), ORB (Vinay et al. 2015), LBP (Pei et al. 2017), SIFT (Sylvia and Kamalaharidharini 2017), and SURF (Cheng et al. 2017). On the other hand, the dimension of the generated hand-crafted feature vector is larger than the dimension of the DF vector. So, there will be a need to use

**Fig. 1** The proposed system architecture



dimensionality reduction techniques before the fusion step. The ICA (Swathi et al. 2018) or PCA (Xiaolin and Yicong 2018) is used for dimensional consistency between the generated features. A fusion network is used to generate the final feature descriptor. The bio-convolving method is executed on the final feature descriptor to improve the system performance against spoof attacks. Finally, the latest layer in the CNN (softmax layer) is used to give the recognition output.

### 3.1 Convolutional neural network

A CNN is a deep learning algorithm that is responsible for taking an input image and assigning learnable weights and biases to various objects in that image. The architecture of a CNN is inspired from the organization of the visual cortex. The CNN architecture is similar to the connectivity pattern of neurons in the human brain. Individual neurons respond to stimuli only in a restricted region of the visual field known as the receptive field. The collection of such fields overlaps to cover the entire visual area. Additionally, an efficient CNN architecture is proposed. The CNNs contain several layers, and each layer performs a specific operation on the input images. Table 1 shows a description of the essential rules of a number of CNN layers (Yuan et al. 2017; Ioffe and Szegedy 2015; Zhang et al. 2016; Yakopcic et al. 2017; Theodoridis and Koutroumbas 2008; Hasnat et al. 2017). Table 2 provides an explanation of the proposed CNN model with the number and the size of filters for each layer.

### 3.2 Feature extraction

Key-points/features are valuable points that are extracted from an image to give the best definition for an object. Feature extraction can be used in several applications such as object detection, object tracking, and object recognition. Feature extraction is the process of computing the abstraction of the image information and making a local decision at every image point to see if there is a feature in that point or not. In the proposed method, several traditional techniques are examined for hand-crafted feature extraction: HOG (Ali et al. 2017), ORB (Vinay et al. 2015), LBP (Pei et al. 2017), SIFT (Sylvia and Kamalaharidharini 2017), and SURF (Cheng et al. 2017).

### 3.3 Dimensionality reduction

Dimensionality reduction is the process of obtaining a set of principal variables to reduce the number of random variables under consideration. In the proposed method, dimensionality reduction using PCA or ICA is applied to reduce the dimensions of the hand-crafted features to be consistent with the dimensions of the DFs.

#### 3.3.1 Independent component analysis

Let us represent the random observed vector  $\mathbf{X} = [X_1, X_2, \dots, X_m]^T$  whose  $m$  elements are mixtures of  $m$  independent elements of a random vector  $\mathbf{S} = [S_1, S_2, \dots, S_m]^T$  as (Swathi et al. 2018):

**Table 1** Essential rules of CNN layers

CNN layers	Essential rule
Convolutional	Learnable filters are used to compute dot products between the entries of both the filter and the input image. The output feature map $\mathbf{f}_{x,y,k}^{C,l}$ for a particular layer $l$ and an input $\mathbf{f}_{x,y}^{O_p,l-1}$ , can be computed as: $\mathbf{f}_{x,y,k}^{C,l} = \mathbf{w}_k^T \mathbf{f}_{x,y}^{O_p,l-1} + b_k^l$ where $\mathbf{w}_k^l$ is the shared weights, $b_k^l$ is the bias and $C$ denotes convolution. $O_p$ represents the input image, for $l = 1$ , while it represents convolution, pooling or activation, for $l > 1$
Max pooling	Max pooling is performed by computing the maximum value in a local spatial neighborhood and then reducing the spatial resolution: $\mathbf{f}_{x,y,k}^{P,l} = \max_{(m,n) \in N_{x,y}} \mathbf{f}_{m,n,k}^{O_p,l-1}$ where the pooling operation is denoted by $P$ , and the local spatial neighborhood of $(x, y)$ coordinate is denoted by $N_{x,y}$ .
Batch normalization	It is used for normalizing the activations of the previous layer, training the network faster, making weights easier to be initialized and simplifying the creation of deeper networks.
Residual learning block “ResBL”	It is used to optimize the loss of CNNs in an easy way. The output of a residual block $R$ can be expressed as: $\mathbf{f}_{x,y,k}^{R,l} = \mathbf{f}_{x,y}^{O_p,l-q} + F\left(\mathbf{f}_{x,y}^{O_p,l-q}, \{\mathbf{w}_k\}\right)$ where $\mathbf{f}_{x,y}^{O_p,l-q}$ is the input feature map, $F(\cdot)$ is the residual mapping to be learned and $q$ is the total number of stacked layers
Depth concatenation	It is used to increase the depth of the feature map by concatenating the output filter banks of a number of layers into a single output vector
Feature normalization	It is used to ensure that all features have equal contributions to the cost function. Normalized features $\mathbf{f}_i^{N_r}$ to the softmax loss will be provided as $\mathbf{f}^{N_r} = \frac{\mathbf{f}^{O_p} - \mu}{\sqrt{\sigma^2}}$ , where $\mu$ and $\sigma^2$ represent the mean and variance, respectively.
Softmax loss	It is used for computing the loss. The form of computing softmax loss is: $L_{softmax} = - \sum_{i=1}^N \log \frac{e^{\mathbf{w}_j^T \mathbf{f}_i + b_j}}{\sum_{j=1}^K e^{\mathbf{w}_j^T \mathbf{f}_i + b_j}}$ where $\mathbf{f}_i$ denotes features and $y_i$ is the true class label of the image. $\mathbf{w}_j$ and $b_j$ are the weights and bias of the $j$ th class, respectively. $N$ is the number of training samples and $K$ is the number of classes.

$$\mathbf{X} = \mathbf{AS} \quad (1)$$

where  $\mathbf{A}$  denotes an  $m \times m$  mixing and  $j = 1, 2, \dots, m$ . The main target of the ICA is to find the non-mixing matrix  $\mathbf{W}$  (i.e., the inverse of  $\mathbf{A}$ ) that will give  $\mathbf{Y}$ . The computation of  $\mathbf{S}$  is illustrated in Eq. (2) (Swathi et al. 2018):

$$\mathbf{Y} = \mathbf{WX} \cong \mathbf{S} \quad (2)$$

Finally, the number of independent components is determined to be equal to the dimension of the deep feature vector, such that the fusion process can be performed correctly.

### 3.3.2 Principal component analysis

The PCA is a popular technique that is used for expressing and representing data in such a way to show similarities and differences. It is a powerful tool that can deal with data of high dimensions. It is applied in image processing applications to compress data without loss of important information. As described in Fig. 2, the PCA starts with

computing the covariance matrix as illustrated in Eq. (3) (Xiaolin and Yicong 2018):

$$\text{cov}(\mathbf{X}, \mathbf{Y}) = \mathbf{A} = \frac{\sum_{i=1}^n (X_i - X')(Y_i - Y')}{(n - 1)} \quad (3)$$

where  $X'$  and  $Y'$  are the mean values of  $\mathbf{X}$  and  $\mathbf{Y}$ , respectively. From the covariance matrix, the eigenvalues are computed according to Eq. (4) (Xiaolin and Yicong 2018):

$$|\mathbf{A} - \lambda \mathbf{I}| = 0 \quad (4)$$

where “ $\mathbf{A}$ ”, “ $\mathbf{I}$ ” and “ $\lambda$ “ are the covariance matrix, the identity matrix and the eigenvalues, respectively. Furthermore, the eigenvector “ $\mathbf{E}$ ” is computed as (Xiaolin and Yicong 2018):

$$[\mathbf{A} - \lambda \mathbf{I}] [\mathbf{E}] = \mathbf{0} \quad (5)$$

The principal components are formed from the calculated eigenvectors as shown in Eq. (6) (Xiaolin and Yicong 2018):

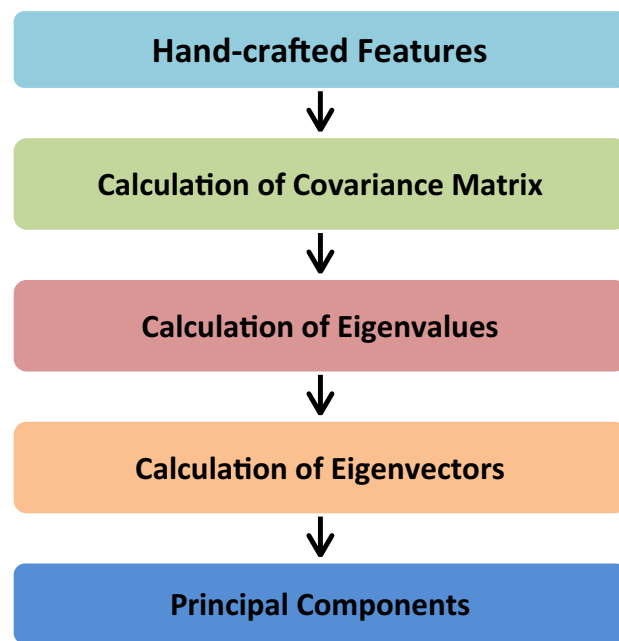
$$\text{Principal components} = [\mathbf{e}_1, \mathbf{e}_2, \mathbf{e}_3, \dots, \mathbf{e}_n] \quad (6)$$

**Table 2** The proposed CNN model

Layer name	No. of filters	Filter size	Stride size	Padding size
Conv1	64	$7 \times 7 \times 3$	$2 \times 2$	$3 \times 3$
ReLU	n/a	n/a	n/a	n/a
Max pooling	1	$3 \times 3$	$2 \times 2$	$1 \times 1$
			Batch normalization	Batch normalization
Conv2	64	$1 \times 1 \times 64$	$1 \times 1$	0
ReLU	n/a	n/a	n/a	n/a
Conv3	128	$3 \times 3 \times 64$	$1 \times 1$	$1 \times 1$
ReLU	n/a	n/a	n/a	n/a
Max pooling	1	$3 \times 3$	$2 \times 2$	$1 \times 1$
ResBL	1	$3 \times 3 \times 64$	$1 \times 1$	$1 \times 1$
Conv4	192	$3 \times 3 \times 64$	$1 \times 1$	$1 \times 1$
ReLU	n/a	n/a	n/a	n/a
Max pooling	1	$3 \times 3$	$1 \times 1$	$1 \times 1$
ResBL	1	$3 \times 3 \times 64$	$1 \times 1$	$1 \times 1$
Conv5	64	$1 \times 1 \times 192$	$1 \times 1$	0
ReLU	n/a	n/a	n/a	n/a
Conv6	96	$1 \times 1 \times 192$	$1 \times 1$	0
ReLU	n/a	n/a	n/a	n/a
Conv7	128	$3 \times 3 \times 96$	$1 \times 1$	$1 \times 1$
ReLU	n/a	n/a	n/a	n/a
Conv8	16	$1 \times 1 \times 192$	$1 \times 1$	0
ReLU	n/a	n/a	n/a	n/a
Conv9	32	$5 \times 5 \times 16$	$1 \times 1$	$2 \times 2$
ReLU	n/a	n/a	n/a	n/a
Max pooling	1	$3 \times 3$	$1 \times 1$	$1 \times 1$
Conv10	32	$1 \times 1 \times 192$	$1 \times 1$	0
ReLU	n/a	n/a	n/a	n/a
			Depth concatenation	Depth concatenation of 4 inputs
Conv11	128	$1 \times 1 \times 256$	$1 \times 1$	0
ReLU	n/a	n/a	n/a	n/a
Conv12	128	$1 \times 1 \times 256$	$1 \times 1$	0
ReLU	n/a	n/a	n/a	n/a
Conv13	192	$3 \times 3 \times 128$	$1 \times 1$	$1 \times 1$
ReLU	n/a	n/a	n/a	n/a
Conv14	32	$1 \times 1 \times 256$	$1 \times 1$	0
ReLU	n/a	n/a	n/a	n/a
Conv15	96	$5 \times 5 \times 32$	$1 \times 1$	$2 \times 2$
ReLU	n/a	n/a	n/a	n/a
Max pooling	1	$3 \times 3$	$1 \times 1$	$1 \times 1$
Conv16	64	$1 \times 1 \times 256$	$1 \times 1$	0
ReLU	n/a	n/a	n/a	n/a
			Depth concatenation	Depth concatenation of 4 inputs
Conv17	192	$1 \times 1 \times 480$	$1 \times 1$	0
ReLU	n/a	n/a	n/a	n/a
Conv18	96	$1 \times 1 \times 480$	$1 \times 1$	0
ReLU	n/a	n/a	n/a	n/a
Conv19	208	$3 \times 3 \times 96$	$1 \times 1$	$1 \times 1$
ReLU	n/a	n/a	n/a	n/a

**Table 2** (continued)

Layer name	No. of filters	Filter size	Stride size	Padding size
Conv20	16	$1 \times 1 \times 480$	$1 \times 1$	0
ReLU	n/a	n/a	n/a	n/a
Conv21	48	$5 \times 5 \times 16$	$1 \times 1$	$2 \times 2$
ReLU	n/a	n/a	n/a	n/a
Max pooling	1	$3 \times 3$	$1 \times 1$	$1 \times 1$
Conv22	64	$1 \times 1 \times 480$	$1 \times 1$	0
ReLU	n/a	n/a	n/a	n/a
			Depth concatenation	Depth concatenation of 4 inputs
Max pooling	1	$3 \times 3$	$2 \times 2$	0
			Dropout	40% Drop-out
			Fully-connected layer	1000 Fully-connected layer
			Feature normalization	Feature normalization
Softmax	n/a	n/a	n/a	n/a

**Fig. 2** PCA algorithm

Finally, the number of principal components is determined to be equal to the dimension of the deep feature vector, such that the fusion process can be performed correctly.

### 3.4 The fusion network

We adopt a fusion network to combine the extracted features into a more representative, reliable, useful and detailed facial descriptor. This network consists of two layers: *local* and *fusion* layers. The *local* layer is composed of two parallel CNNs. If we consider that  $\mathbf{F}^{(i)}(\cdot)$  represents

the DF vector, which is extracted from a CNN  $i$ , then the output of the *fusion* layer could be computed as illustrated in Eq. (7):

$$\text{Final facial descriptor} = \left( \sum_{i=1}^n \mathbf{W}_f^{(i)} \cdot \mathbf{F}^{(i)}(\cdot) + b_f \right) \quad (7)$$

where  $b_f$  and  $\mathbf{W}_f^{(i)}$  are the fusion layer bias and weights, and  $n$  represents the number of CNNs (in this case  $n = 2$ ).

### 3.5 The bio-convolving method

This method (Patel et al. 2015) adopts a convolution approach that leads to generating cancelable biometric templates. A transformed sequence  $f(i)$ ,  $i = 1, \dots, F$ , is obtained using an original sequence  $r(i)$ ,  $i = 1, \dots, F$ , through a convolution with a random kernel  $h(i)$ .

$$f(i) = r(i) * h(i) \quad (8)$$

## 4 Experimental results

This section reveals the effectiveness of the proposed method using various biometric traits that include face, iris, fingerprint, palm print, and ear. We performed experiments on various datasets, which are Point and Shoot Face Recognition Challenge (PaSC) (Beveridge et al. 2013) for FR, the Institute of Automation, Chinese Academy of Sciences (CASIA)-IrisV3 (2018) for IR, CASIA Fingerprint (2018) for fingerprint recognition, College of Engineering—Pune (COEP) Palm Print (2018) for palm print recognition, and Mathematical Analysis of Images (AMI) Ear (2018) for ear recognition. Furthermore, comparisons with the state-of-the-art methods are provided in terms of

**Table 3** Equations of the performance metrics

Performance metric	Equation
Accuracy	$\frac{TP+TN}{TP+FP+FN+TN}$
Specificity	$\frac{TN}{FP+TN}$
Precision	$\frac{TP}{TP+FP}$
Recall	$\frac{TP}{TP+FN}$
$F_{\text{score}}$	$\frac{2 \times \text{Recall} \times \text{Precision}}{\text{Recall} + \text{Precision}}$

*TP* true positive, *FN* false negative, *FP* false positive, and *TN* true negative

**Table 4** The platform specifications

System	Specifications
Type	64-bit Win 10
Processor	Intel Xeon 5670, 12 cores
Graphics card	NVIDIA GeForce GTX 1070
Installed memory (RAM)	48G memory

the performance metrics presented in Table 3. Table 4 shows the specifications of the experiments platform. We exploited the stochastic gradient descent with momentum (SGDM) method to train the novel CNN model and the momentum is set to 0.9. Moreover, we apply  $L_2$  regularization with the weight decay set to  $5 \times 10^{-4}$ . We begin the CNN training with a learning rate of 0.1 and stop the training after 5 epochs. An epoch is a full training cycle on the entire training dataset. The mini-batch size is adjusted to 64. The experimental results are obtained using 5-fold cross validation. The network accuracy is monitored during training by specifying the validation data and the validation frequency. The data is shuffled every epoch. The software trains the network on the training data and calculates the accuracy on the validation data at regular intervals during training. The validation data is not used to update the network weights. Finally, the network is trained using the architecture that is defined by the layers, the training data, and the training options. Tables 5, 6, and 7 describe the effect of different hyper-parameters on the recognition performance using various optimization algorithms: SGDM, root mean square propagation (RMS prop), and adaptive moment estimation (Adam), respectively.

The experimental results of the proposed method are organized as FR results, IR results, fingerprint recognition results, palm print recognition results, and ear recognition results. The performance of the proposed method is studied using various algorithms for hand-crafted feature

extraction. The PCA or the ICA is applied to reduce the dimensions of the extracted hand-crafted features to be consistent with the dimensions of the DFs. The proposed CNN model is used for DF extraction. In addition, comparisons with the state-of-the-art CNNs are presented for more validation of the effectiveness of the proposed CNN.

#### 4.1 Face recognition results

Table 8 presents the performance of the proposed FR method. From the results, the utilization of HOG algorithm for feature extraction and ICA for dimensionality reduction achieves remarkable results.

Table 9 provides a comparison between the proposed CNN and the state-of-the-art CNNs. The proposed CNN achieves a promising performance compared to the other CNNs. Figure 3 shows the ROC plot for the proposed and CoCo loss CNN models. A graphical comparison between various CNNs in terms of recognition accuracy for FR is given in Fig. 4.

#### 4.2 Iris recognition results

Table 10 presents the experimental results of IR. The results show that the utilization of the LBPs algorithm for feature extraction and the ICA algorithm for dimensionality reduction achieves promising results on CASIA-IrisV3 dataset.

Table 11 shows a comparison between the proposed method and the state-of-the-art IR methods. The proposed method achieves a superior recognition performance. Figure 5 displays the ROC plot for the proposed and the CoCo loss CNN models. Figure 6 illustrates a graphical comparison between different CNN architectures for IR.

#### 4.3 Fingerprint recognition results

Table 12 summarizes the experimental results of the fingerprin recognition using different methods for feature extraction and dimensionality reduction. The experimental results reveal that the utilization of the SIFT for feature extraction and the ICA for dimensionality reduction gives superior recognition results.

Table 13 presents a comparison between the performance of the proposed method and the state-of-the-art methods for fingerprint recognition. The results indicate that the proposed method has a superior performance. Figure 7 demonstrates the ROC plots for the proposed and the CoCo loss CNN models. In addition, the recognition accuracy levels obtained with different CNNs for fingerprin recognition are illustrated graphically in Fig. 8.

**Table 5** The effect of hyper-parameters on the recognition performance using SGDM optimization algorithm

Hyper-parameters		Performance metrics				
Mini-batch size	Learning rate	Accuracy (%)	Specificity (%)	Precision (%)	Recall (%)	$F_{\text{score}} (\%)$
32	0.1	94.58	94.68	92.26	93.57	92.91
	0.01	93.89	93.96	91.48	92.73	92.1
	0.001	89.24	89.35	86.82	88.17	87.48
64	0.1	<b>97.14</b>	<b>97.23</b>	<b>94.93</b>	<b>96.23</b>	<b>95.57</b>
	0.01	96.92	97.05	94.51	95.85	95.17
	0.001	95.66	95.74	93.34	94.58	93.95
128	0.1	95.27	95.39	92.94	94.24	93.58
	0.01	92.74	92.86	91.06	91.38	91.21
	0.001	92.51	92.63	90.83	91.17	90.99

Best results are shown in bold

**Table 6** The effect of hyper-parameters on the recognition performance using RMS prop optimization algorithm

Hyper-parameters		Performance metrics				
Mini-batch size	Learning rate	Accuracy (%)	Specificity (%)	Precision (%)	Recall (%)	$F_{\text{score}} (\%)$
32	0.1	94.84	94.97	92.35	93.89	93.11
	0.01	91.96	92.08	89.81	90.89	90.35
	0.001	88.85	88.94	86.31	87.86	87.07
64	0.1	<b>96.77</b>	<b>96.86</b>	<b>94.23</b>	<b>95.74</b>	<b>94.97</b>
	0.01	96.53	96.62	94.03	95.49	94.75
	0.001	93.68	93.76	91.5	92.27	91.88
128	0.1	95.26	95.35	92.71	94.28	93.48
	0.01	94.19	94.27	91.64	93.12	92.37
	0.001	93.42	93.49	90.83	92.34	91.57

Best results are shown in bold

**Table 7** The effect of hyper-parameters on the recognition performance using Adam optimization algorithm

Hyper-parameters		Performance metrics				
Mini-batch size	Learning rate	Accuracy (%)	Specificity (%)	Precision (%)	Recall (%)	$F_{\text{score}} (\%)$
32	0.1	94.25	94.37	91.86	93.46	92.65
	0.01	90.59	90.67	88.37	89.61	88.99
	0.001	88.89	88.99	86.49	88.07	87.27
64	0.1	<b>96.84</b>	<b>96.96</b>	<b>94.48</b>	<b>95.91</b>	<b>95.18</b>
	0.01	96.58	96.68	94.15	95.78	94.95
	0.001	94.82	94.93	92.63	93.71	93.17
128	0.1	94.95	95.06	92.56	94.13	93.33
	0.01	95.32	95.45	92.95	94.48	93.7
	0.001	93.59	93.67	91.15	92.74	91.93

Best results are shown in bold

**Table 8** The experimental results of the proposed FR method

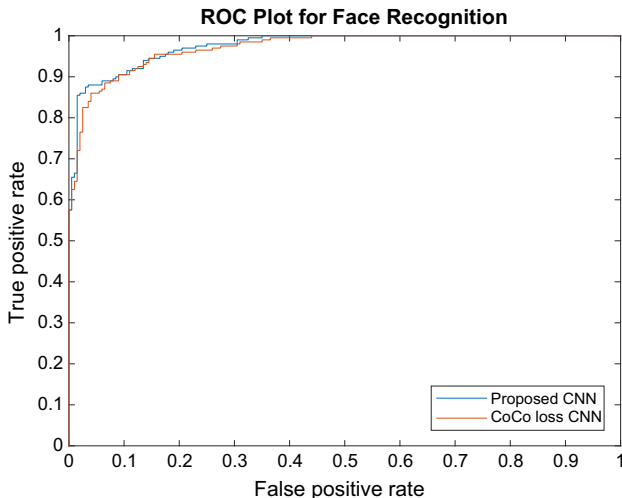
FE algorithm	DR method	Accuracy (%)	Specificity (%)	Precision (%)	Recall (%)	$F_{\text{score}} (%)$
SURF	PCA	93.14	93.23	91.34	92.34	91.83
SIFT		94.23	94.36	92.45	93.53	92.98
LBP		94.76	94.85	92.97	93.83	93.39
ORB		94.57	94.66	92.75	93.81	93.27
HOG		95.07	95.15	93.22	94.26	93.73
SURF	ICA	95.04	95.12	93.15	94.22	93.68
SIFT		95.3	95.41	93.43	94.51	93.96
LBP		96	96.11	94.16	95.26	94.7
ORB		95.83	95.92	93.95	95.06	94.5
HOG		<b>96.69</b>	<b>96.77</b>	<b>94.88</b>	<b>95.94</b>	<b>95.4</b>

Best results are shown in bold

**Table 9** Comparison between the proposed and the state-of-the-art CNNs for FR

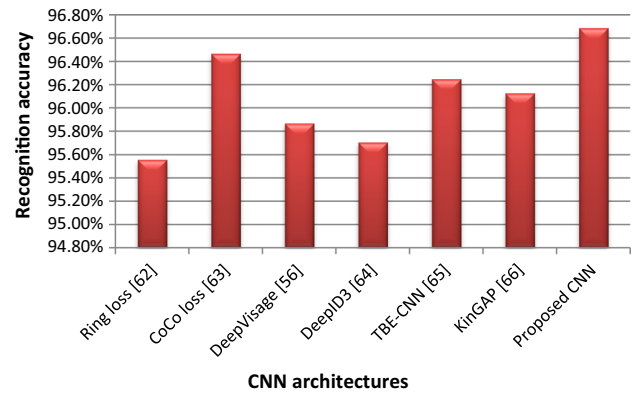
CNN	Accuracy (%)	Specificity (%)	Precision (%)	Recall (%)	$F_{\text{score}} (%)$
Ring loss (Zheng et al. 2018)	95.56	95.64	93.77	94.83	94.29
CoCo loss (Liu et al. 2017)	96.47	96.55	94.64	95.78	95.2
DeepVisage (Hasnat et al. 2017)	95.87	95.97	94.09	95.14	94.61
DeepID3 (Sun et al. 2015)	95.71	95.8	93.84	94.92	94.37
TBE-CNN (Ding and Tao 2017)	96.25	96.34	94.47	95.56	95.01
KinGAP (Sh et al. 2016)	96.13	96.28	94.43	95.48	94.95
Proposed CNN	<b>96.69</b>	<b>96.77</b>	<b>94.88</b>	<b>95.94</b>	<b>95.4</b>

Best results are shown in bold

**Fig. 3** The ROC plot of the proposed and the CoCo loss models for FR

#### 4.4 Palm print recognition results

Table 14 displays the palm print recognition results using LBPs as a feature extraction method with PCA for

**Fig. 4** Graphical comparison between various CNNs for FR

dimensionality reduction. This scheme gives the best performance.

Table 15 summarizes the experimental results for palm print recognition based on the proposed and the state-of-the-art methods. It is shown that the proposed method has a better performance. Figure 9 displays the ROC plots for the proposed and DeepVisage CNN models. Also, for palm print recognition, Fig. 10 shows the recognition accuracy using various CNN architectures.

**Table 10** The experimental results of the proposed IR method

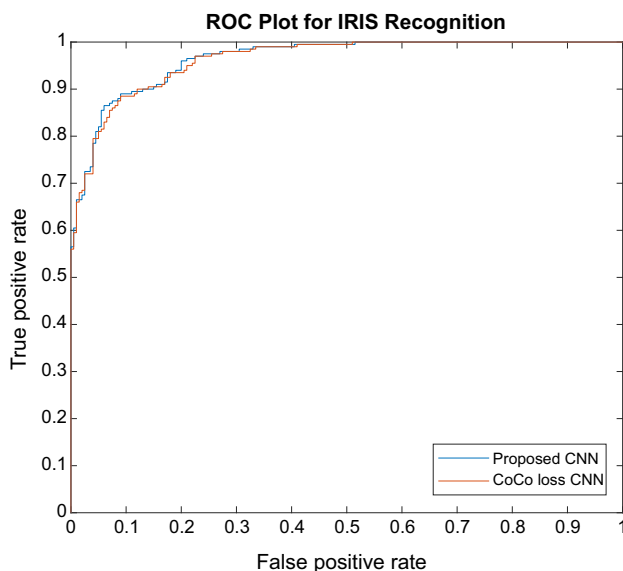
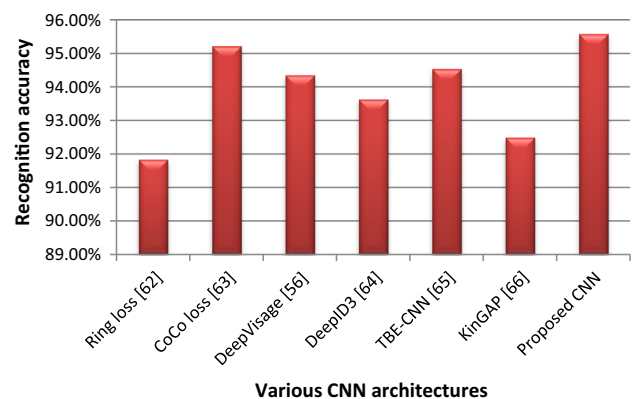
Feature extraction algorithm	Dimensionality reduction method	Accuracy (%)	Specificity (%)	Precision (%)	Recall (%)	$F_{\text{score}} (%)$
SURF	PCA	90.73	90.78	87.94	89.98	88.94
SIFT		92.82	92.94	90.16	92.14	91.13
LBP		94.35	94.47	91.68	93.66	92.66
ORB		93.16	93.22	90.47	92.39	91.41
HOG		93.66	93.79	90.93	92.99	91.94
SURF	ICA	93.63	93.71	90.96	92.96	91.94
SIFT		93.89	93.95	91.15	93.17	92.14
LBP		<b>95.59</b>	<b>95.68</b>	<b>92.82</b>	<b>94.87</b>	<b>93.83</b>
ORB		94.42	94.51	91.75	93.73%	92.72
HOG		95.28	95.39	92.69	94.65	93.65

Best results are shown in bold

**Table 11** Comparison between the proposed and the state-of-the-art IR CNNs

CNN	Accuracy (%)	Specificity (%)	Precision (%)	Recall (%)	$F_{\text{score}} (%)$
Ring loss (Zheng et al. 2018)	91.84	91.94	89.85	90.65	90.24
CoCo loss (Liu et al. 2017)	95.23	95.36	93.34	94.03	93.68
DeepVisage (Hasnat et al. 2017)	94.36	94.46	92.33	93.18	92.75
DeepID3 (Sun et al. 2015)	93.64	93.68	91.54	92.37	91.95
TBE-CNN (Ding and Tao 2017)	94.55	94.64	92.48	93.26	92.87
KinGAP (Sh et al. 2016)	92.5	92.57	90.45	91.26	90.85
Proposed CNN	<b>95.59</b>	<b>95.68</b>	<b>92.82</b>	<b>94.87</b>	<b>93.83</b>

Best results are shown in bold

**Fig. 5** The ROC plots of the proposed and the CoCo loss CNNs for IR**Fig. 6** Graphical comparison between various CNNs for IR

#### 4.5 Ear recognition results

Table 16 collects the results for ear recognition based on different methods for feature extraction and dimensionality reduction. The results ensure that the utilization of SIFT and ICA gives superior performance.

Table 17 provides a comparison between the proposed methods and different state-of-the-art methods for ear

**Table 12** The experimental results of the proposed fingerprint recognition method

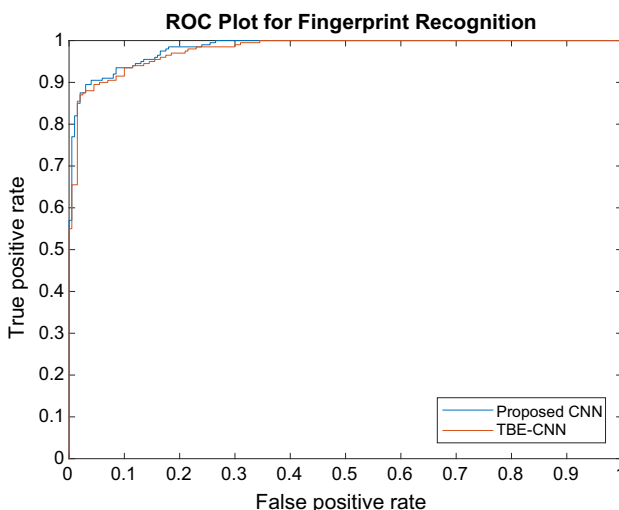
Feature extraction algorithm	Dimensionality reduction method	Accuracy (%)	Specificity (%)	Precision (%)	Recall (%)	$F_{\text{score}} (%)$
SURF	PCA	92.72	92.85	90.84	91.64	91.23
SIFT		95.06	95.17	93.25	94.05	93.64
LBP		94.09	94.22	92.34	93.08	92.7
ORB		93.45	93.59	91.76	92.47	92.11
HOG		94.74	94.88	93.08	93.77	93.42
SURF	ICA	94.93	95.08	93.11	93.95	93.52
SIFT		<b>97.34</b>	<b>97.47</b>	<b>95.57</b>	<b>96.32</b>	<b>95.94</b>
LBP		96.56	96.68	94.75	95.55	95.14
ORB		96.25	96.37	94.5	95.26	94.87
HOG		95.63	95.76	93.83	94.64	94.23

Best results are shown in bold

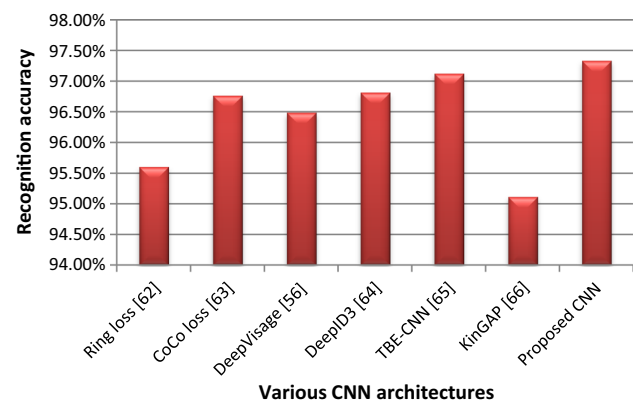
**Table 13** Comparison between the proposed and the state-of-the-art CNNs for fingerprint recognition

CNN	Accuracy (%)	Specificity (%)	Precision (%)	Recall (%)	$F_{\text{score}} (%)$
Ring loss (Zheng et al. 2018)	95.61	95.73	93.63	94.42	94.02
CoCo loss (Liu et al. 2017)	96.77	96.86	94.84	95.66	95.24
DeepVisage (Hasnat et al. 2017)	96.49	96.57	94.57	95.34	94.95
DeepID3 (Sun et al. 2015)	96.82	96.95	94.88	95.67	95.27
TBE-CNN (Ding and Tao 2017)	97.13	97.26	95.34	96.13	95.73
KinGAP (Sh et al. 2016)	95.12	95.24	93.14	93.93	93.53
Proposed CNN	<b>97.34</b>	<b>97.47</b>	<b>95.57</b>	<b>96.32</b>	<b>95.94</b>

Best results are shown in bold

**Fig. 7** The ROC plots for the proposed and the TBE-CNN Fingerprint recognition models

recognition. The results indicate that the proposed method achieves a more promising performance than those of the other CNN models. Figure 11 displays the ROC plots for the proposed and TBE-CNN models. A graphical

**Fig. 8** Graphical comparison between various CNNs for Fingerprint recognition

comparison between various CNNs in terms of recognition accuracy is presented in Fig. 12.

#### 4.6 Evaluation of cancelable biometric methods

The proposed method uses the bio-convolving encryption to provide protection of biometric data with a slight

**Table 14** The experimental results of the proposed palm print method

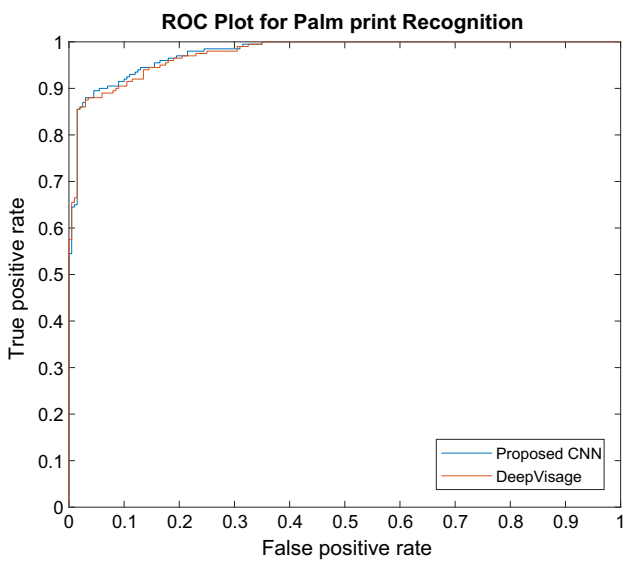
Feature extraction algorithm	Dimensionality reduction method	Accuracy (%)	Specificity (%)	Precision (%)	Recall (%)	$F_{\text{score}} (\%)$
SURF	PCA	92.71	92.83	90.84	91.63	91.23
SIFT		<b>96.11</b>	<b>96.25</b>	<b>94.26</b>	<b>95.06</b>	<b>94.65</b>
LBP		94.13	94.24	92.24	93.05	92.64
ORB		95.82	95.97	94.4	94.77	94.58
HOG		94.47	94.55	92.54	93.34	92.93
SURF	ICA	94.45	94.58	92.53	93.36	92.94
SIFT		95.63	95.72	93.65	94.45	94.04
LBP		93.37	93.49	91.51	92.28	91.89
ORB		95.31	95.43	93.47	94.24	93.85
HOG		93.55	93.68	91.63	92.46	92.04

Best results are shown in bold

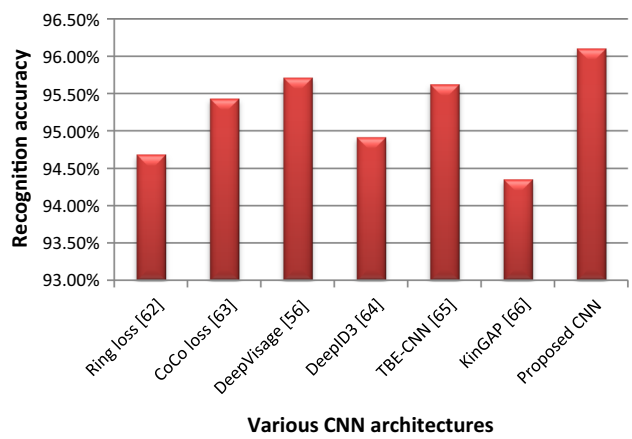
**Table 15** Comparison between the proposed and the state-of-the-art CNNs for palm print recognition

CNN	Accuracy (%)	Specificity (%)	Precision (%)	Recall (%)	$F_{\text{score}} (\%)$
Ring loss (Zheng et al. 2018)	94.69	94.78	92.67	93.42	93.04
CoCo loss (Liu et al. 2017)	95.44	95.57	93.43	94.28	93.85
DeepVisage (Hasnat et al. 2017)	95.72	95.81	93.66	94.43	94.04
DeepID3 (Sun et al. 2015)	94.92	95.07	92.98	93.74	93.35
TBE-CNN (Ding and Tao 2017)	95.63	95.75	93.62	94.45	94.03
KinGAP (Sh et al. 2016)	94.36	94.44	92.36	93.12	92.73
Proposed CNN	<b>96.11</b>	<b>96.25</b>	<b>94.26</b>	<b>95.06</b>	<b>94.65</b>

Best results are shown in bold

**Fig. 9** The ROC plots of the proposed and the DeepVisage models for palm print recognition

degradation in the system accuracy. Table 18 illustrates the change in the recognition accuracy of the proposed method

**Fig. 10** Graphical comparison between various CNNs for Palm print recognition method

after applying the bio-convolving and Bloom filter (Rathgeb et al. 2015) methods. Table 6 shows that the recognition accuracy is slightly affected after applying the bio-convolving method. In addition, Fig. 13 shows a graphical comparison between different cancelable recognition techniques and their influence on the recognition accuracy.

**Table 16** The experimental results of the proposed ear recognition method

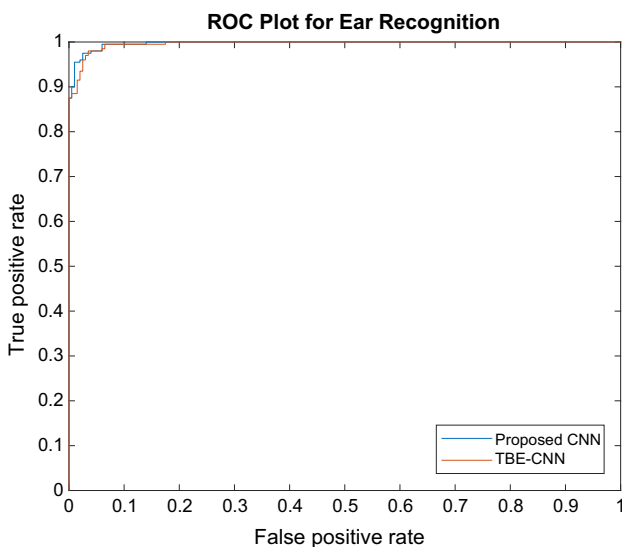
Feature extraction algorithm	Dimensionality reduction method	Accuracy (%)	Specificity (%)	Precision (%)	Recall (%)	$F_{\text{score}} (%)$
SURF	PCA	95.98	96.11	94.25	94.95	94.59
SIFT		97.74	97.86	95.93	96.64	96.28
LBP		97.35	97.46	95.55	96.25	95.89
ORB		97.02	97.16	95.13	95.92	95.52
HOG		97.62	97.74	95.85	96.54	96.19
SURF	ICA	97.64	97.77	95.83	96.58	96.2
SIFT		<b>99.22</b>	<b>99.31</b>	<b>97.48</b>	<b>98.16</b>	<b>97.81</b>
LBP		98.54	98.67	96.76	97.43	97.09
ORB		98.41	98.52	96.62	97.35	96.98
HOG		97.93	98.14	96.25	96.95	96.59

Best results are shown in bold

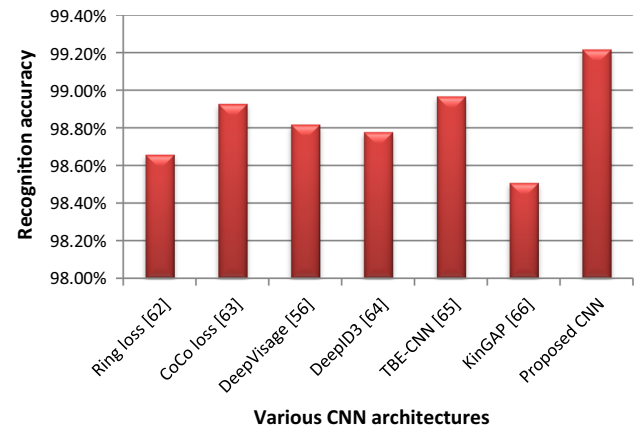
**Table 17** Comparison between the proposed and the state-of-the-art ear recognition CNNs

CNN	Accuracy (%)	Specificity (%)	Precision (%)	Recall (%)	$F_{\text{score}} (%)$
Ring loss (Zheng et al. 2018)	98.66	98.78	96.82	97.56	97.18
CoCo loss (Liu et al. 2017)	98.93	99.04	96.97	97.73	97.34
DeepVisage (Hasnat et al. 2017)	98.82	98.94	96.98	97.68	97.32
DeepID3 (Sun et al. 2015)	98.78	98.85	96.86	97.55	97.2
TBE-CNN (Ding and Tao 2017)	98.97	99.11	97.04	97.82	97.42
KinGAP (Sh et al. 2016)	98.51	98.62	96.65	97.34	96.99
Proposed CNN	<b>99.22</b>	<b>99.31</b>	<b>97.48</b>	<b>98.16</b>	<b>97.81</b>

Best results are shown in bold

**Fig. 11** The ROC plots for the proposed and the TBE-CNN ear recognition models

It is shown that both techniques have high recognition accuracy for ear recognition but lower values for iris recognition. Furthermore, bio-convolving has higher recognition accuracy for all traits compared to the Bloom filter technique. The difference in recognition accuracy

**Fig. 12** Graphical comparison between various CNNs for ear recognition**Table 18** Recognition accuracies of cancelable biometric recognition methods

Recognition method	Bio-convolving (%)	Bloom filter (%)
Face	96.69	93.17
Iris	95.59	92.79
Fingerprint	97.34	93.73
Palm print	96.11	93.09
Ear	99.22	95.86

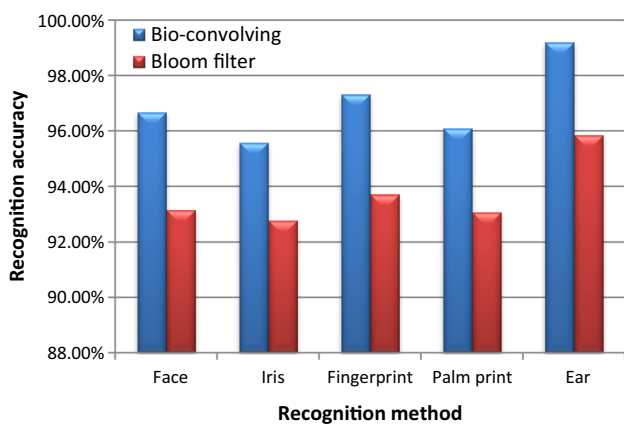


**Fig. 13** Recognition accuracies of cancelable biometric recognition systems

between the two cancelable recognition methods reaches 3.52% for FR, 2.8% for IR, 3.61% for fingerprint recognition, 3.02% for palm print recognition, and 3.36% for ear recognition.

We can verify the ability of the bio-convolving method to provide security and privacy of users' data through performing encryption and decryption operations on a number of images that represent various biometric traits. Figure 14 illustrates the original images, the encrypted images after applying the bio-convolving method, the decrypted images with the same de-convolution mask, and the decrypted images with a slightly different de-convolution mask.

The probability density function (PDF) of the mean square error (MSE) and the normalized absolute error (NAE) for the face, iris, fingerprint, palm print, and ear images are illustrated in Figs. 15, 16, 17, 18, and 19, respectively.

From the Figs. 15:19, it can be noticed that the utilization of the same de-convolution mask in the decryption operation results in low values of MSE and NAE. On the other hand, the utilization of a slightly different mask in the decryption operation results in high values of MSE and

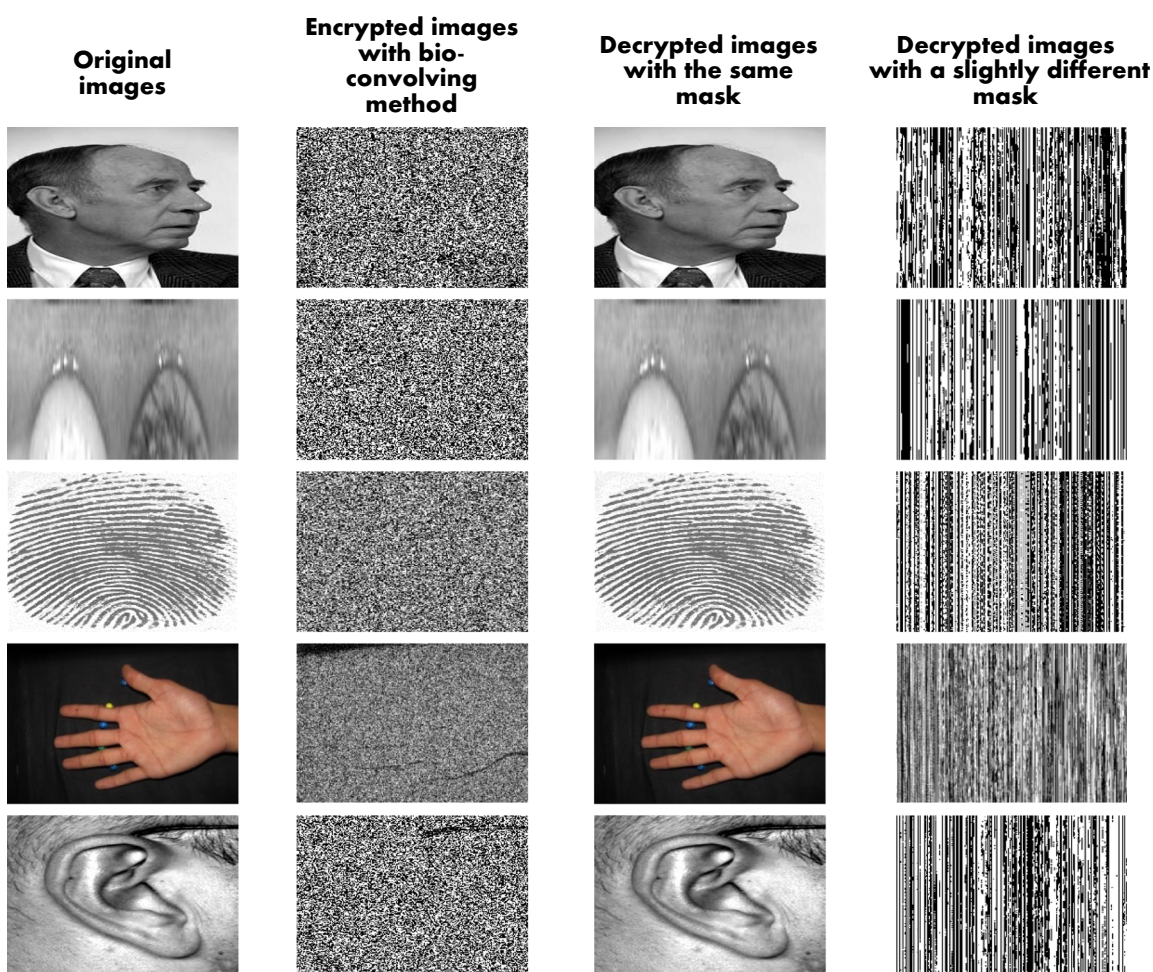


**Fig. 14** Encryption and decryption operations on a number of face, iris, fingerprint, palm print, and ear images using different de-convolution masks

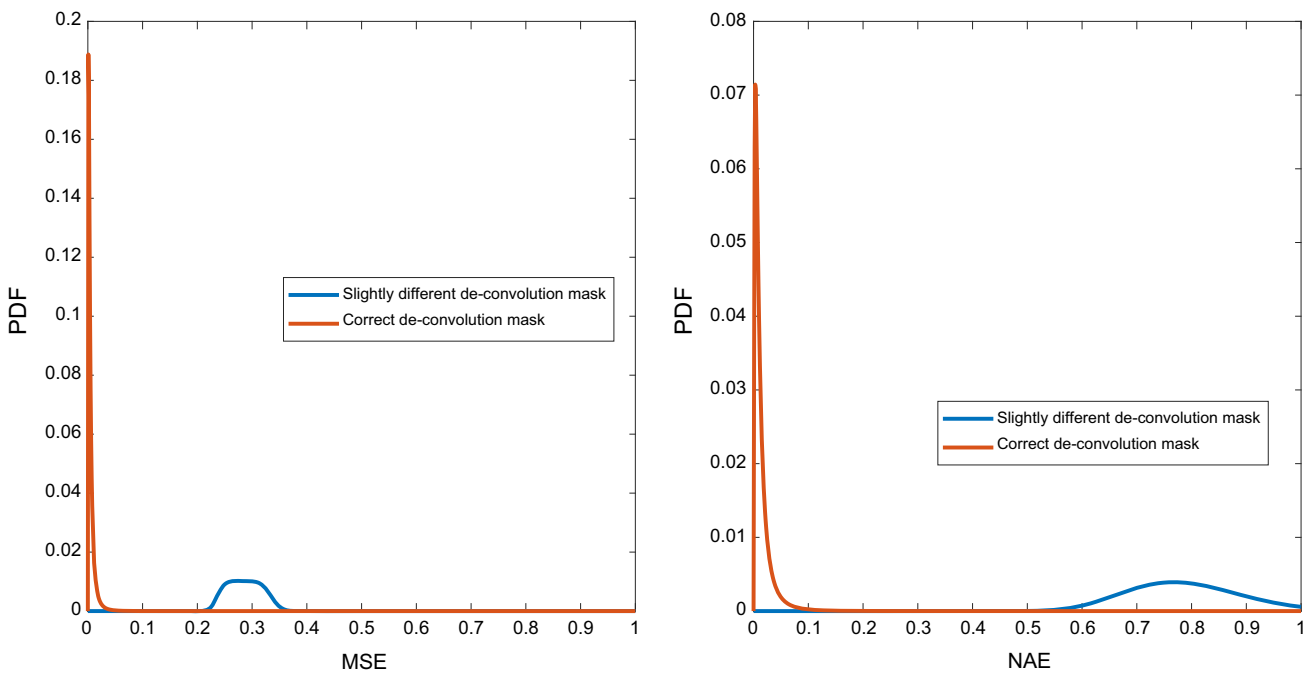


**Fig. 15** The PDFs of MSE and NAE on the face images

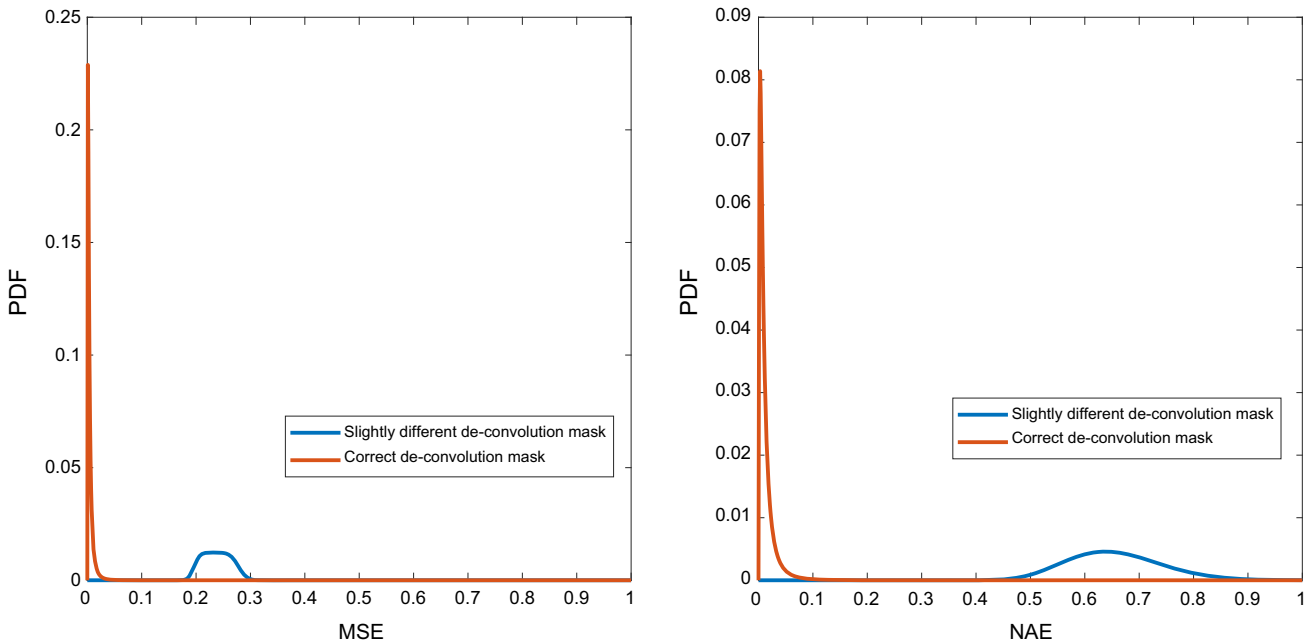


**Fig. 16** The PDFs of MSE and NAE on the iris images

NAE. So, we can say that the bio-convolving method succeeds in providing security and privacy of users' data.

Hence, it is clear that the proposed method achieves a promising performance by taking the advantage of extracting various types of features and combining them into a more efficient descriptor. In addition, the bio-convolving has achieved the required data protection with a slight degradation in the recognition accuracy.

## 5 Conclusion

In this paper, we proposed a new cancelable biometric-based recognition method with a superior performance on various biometric datasets. We have employed depth concatenation and residual layers to construct a novel CNN structure that is used to extract the DFs from biometric images. Consequently, the DFs are combined with another

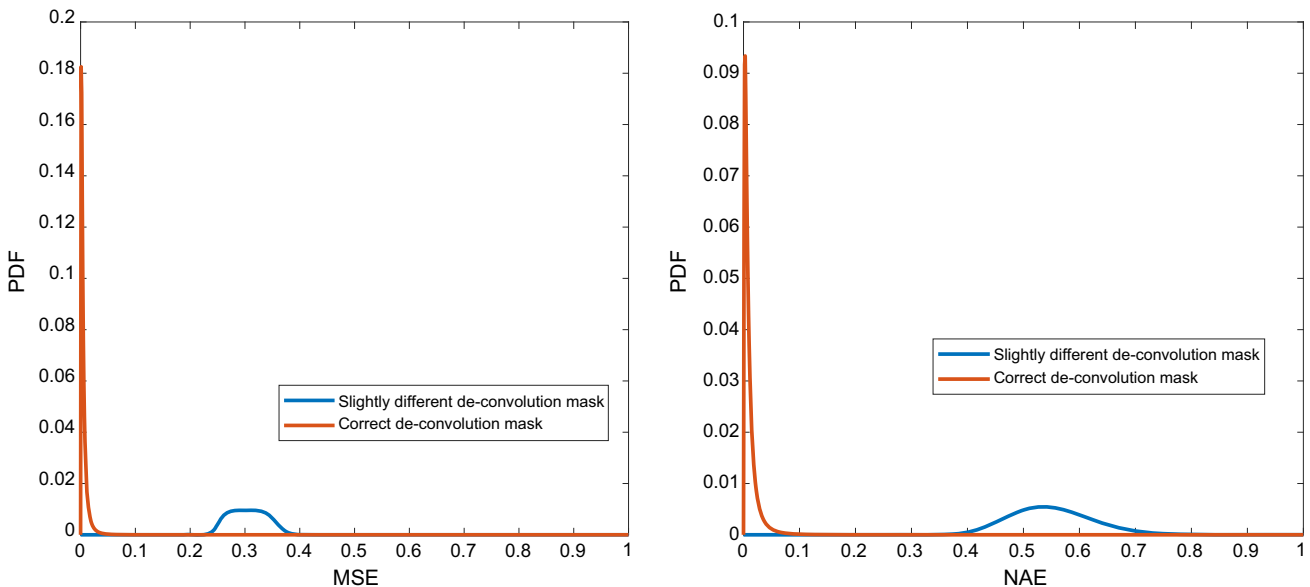


**Fig. 17** The PDFs of MSE and NAE on the fingerprint images

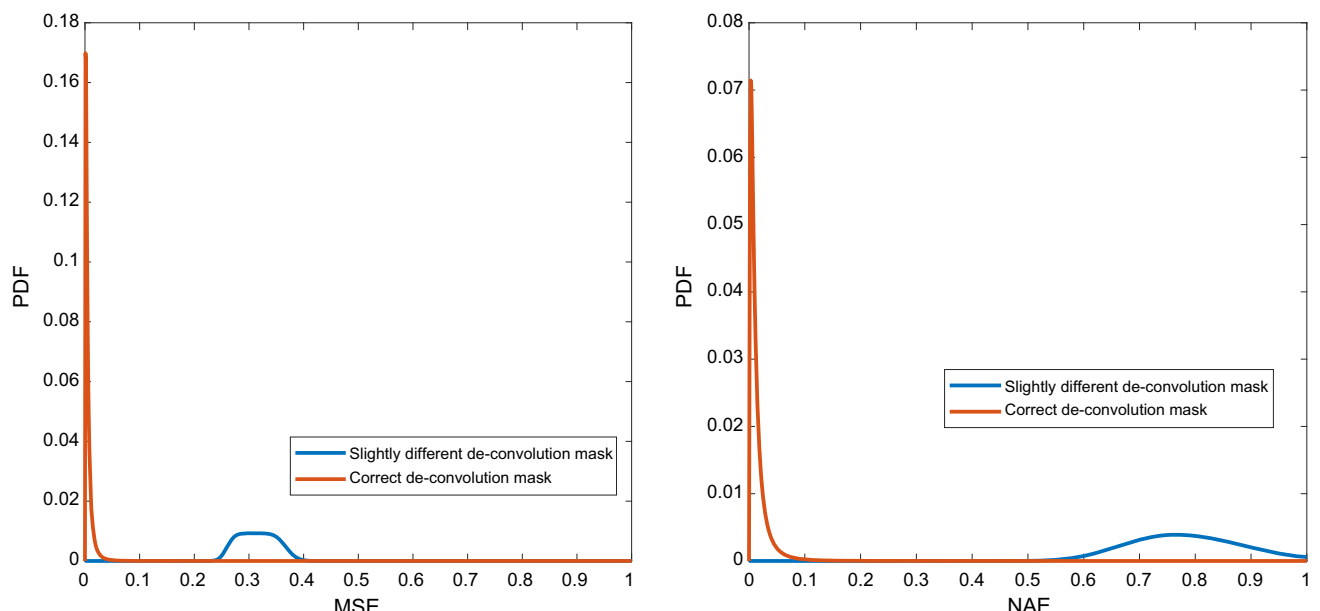


**Fig. 18** The PDFs of MSE and NAE on the palm print images

type of features; hand-crafted features, using a fusion network. Finally, the bio-convolving technique is applied on the final biometric descriptors to maintain the template protection and ensure the users' privacy. In addition, we have studied the effect of varying the mini-batch size and the learning rate on the recognition performance using various optimization algorithms. The experimental results on various datasets demonstrated that the proposed CNN model extracts better DFs than those of the other state-of-

the-art CNN models. The HOG and the ICA are suitable for FR, the LBPs and the ICA are suitable for IR, the SIFT and the ICA are suitable for fingerprint recognition, the SIFT and the PCA are suitable for palm print recognition, and the SIFT and the ICA are suitable for ear recognition. The bio-convolving technique performs better than the Bloom filter in providing cancelability.

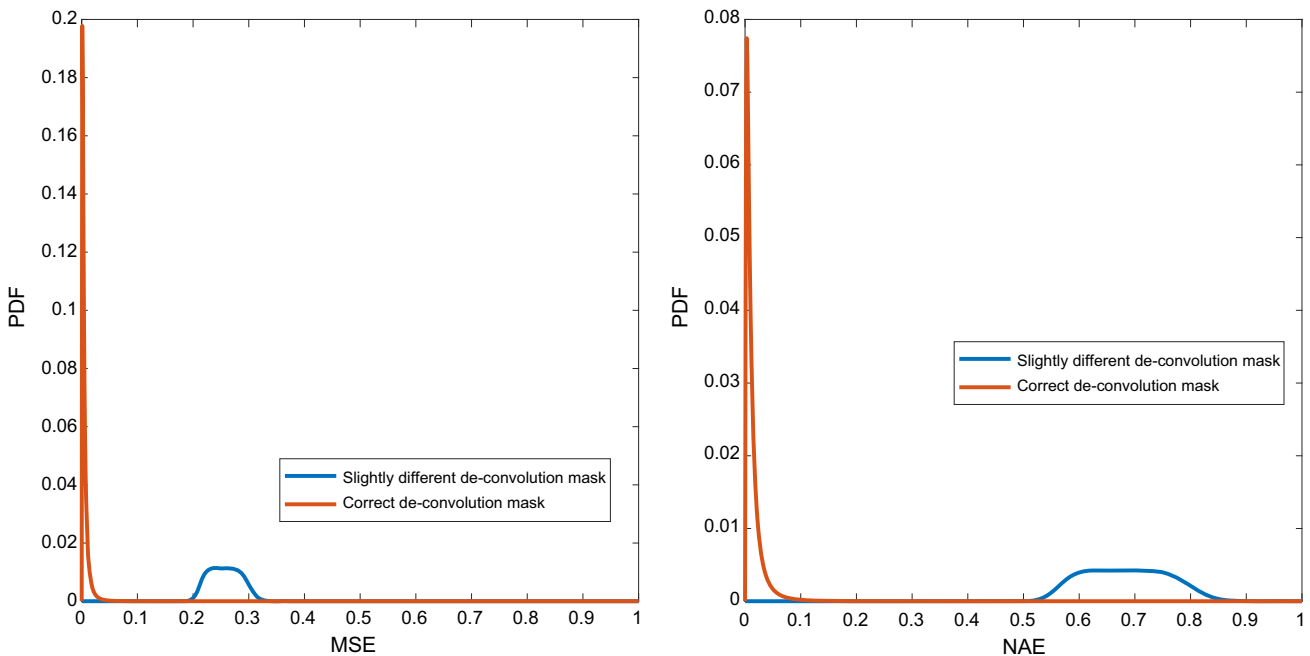


**Fig. 19** The PDFs of MSE and NAE on the ear images

## Compliance with ethical standards

**Conflict of interest** The authors declare that they have no conflict of interest.

**Ethical approval** All procedures performed in studies involving human participants were in accordance with the ethical standards of the institutional and/or national research committee and with the 1964 Helsinki Declaration and its later amendments or comparable ethical standards.

**Informed consent** Informed consent was obtained from all individual participants included in the study.

## References

- Ali H, Jahangir U, Yousuf B, Noor A (2017) Human action recognition using SIFT and HOG method. In: Proceedings of the international conference on information and communication technologies (ICICT), pp 6–10
- AMI ear database (2018), [http://ctim.ulpgc.es/research\\_works/ami\\_ear\\_database/](http://ctim.ulpgc.es/research_works/ami_ear_database/) Accessed Nov 2018
- Bengio Y, Courville A, Vincent P (2013) Representation learning: a review and new perspectives. In: IEEE transactions on pattern analysis and machine intelligence, pp 1798–1828
- Beveridge J, Phillips J, Bolme D, Draper B, Givens G, Lui Y, Teli M, Zhang H, Scruggs W, Bowyer K (2013) The challenge of face recognition from digital point-and-shoot cameras. In: Proceedings of IEEE international conference biometrics, theory, application system, pp 1–8
- Bolle RM, Connell JH, Ratha NK (2002) Biometrics perils and patches. In: Pattern Recognition, pp 2727–2738
- CASIA Fingerprint Image Database Version 5.0, <http://biometrics.idealtest.org/dbDetailForUser.do?id=7>. Accessed Nov 2018
- CASIA-IrisV3 Database (2018), <http://www.cbsr.ia.ac.cn/english/IrisDatabase.asp>. Accessed May 2018
- COEP Palm Print Database (2018) <http://www.coep.org.in/resources/coeppalmprintdatabase.m> Accessed Dec 2018
- Cheng C, Wang X, Li X (2017) UAV image matching based on surf feature and harris corner algorithm. In: Proceedings of the international conference on smart and sustainable city (ICSSC), pp 1–6
- Chin C, Jin A, Ling D (2006) High security iris verification system based on random secret integration. In: Elsevier computer vision and image understanding, pp 169–177
- Connie T, Jin T, Ong M, Ling D (2005) Ling D (2005) An automated palmprint recognition system. Image Vis Comput 23:501–515
- Daugman J (2016) Information theory and the iris code. In: IEEE transactions on information forensics and security, pp 400–409
- Deng W, Yao R, Zhao H, Yang X, Li G (2017a) A novel intelligent diagnosis method using optimal LS-SVM with improved PSO algorithm. Soft Comput 23:2445
- Deng W, Zhao H, Zou L, Li G, Yang X, Wu D (2017b) A novel collaborative optimization algorithm in solving complex optimization problems. Soft Comput 21:4387–4398. <https://doi.org/10.1007/s00500-016-2071-8>
- Ding C, Tao D (2017) Trunk-branch ensemble convolutional neural networks for video-based face recognition. IEEE Trans Pattern Anal Mach Intell 40(4):1002–1014
- Ekinci M, Aykut M (2007) Gabor-based kernel PCA for palmprint recognition. Electr Lett 43:1077–1079
- Emersic Z, Stepec D, Struc V (2017a) Training convolutional neural networks with limited training data for ear recognition in the wild. In: Automatic face gesture recognition, pp 987–994
- Emersic Z, Struc V, Peer P (2017b) Ear recognition: more than a survey. Neurocomputing 255:26–39
- Gangwar A, Joshi A (2016) Deepirisnet: deep iris representation with applications in iris recognition and cross-sensor iris recognition. In: IEEE international conference on image processing (ICIP), pp 2301–2305

- Harjoko A, Hartati S, Dwiyasa H (2009) A method for iris recognition based on 1d coiflet wavelet. In: World academy of science engineering and technology, pp 126–129
- Hasnat A, Bohme J, Milgram J, Gentric S, Chen L (2017) DeepVisage: making face recognition simple yet with powerful generalization Skills. In: Proceedings of the IEEE conference on computer vision and pattern recognition (CVPR), pp 1–12
- Iandola F, Han S, Moskewicz M (2016) SqueezeNet: AlexNet-level accuracy with 50x fewer parameters and <0.5 MB model size. In: arXiv preprint [arXiv:1602.07360](https://arxiv.org/abs/1602.07360)
- Ignat A, Luca M, Ciobanu A (2013) Iris features using dual tree complex wavelet transform in texture evaluation for biometrical identification. In: IEEE E-health and bioengineering conference, pp 1–4
- Ioffe S, Szegedy C (2015) Batch normalization: accelerating deep network training by reducing internal covariate shift. In: Proceedings of the international conference on machine learning (ICML). [arXiv:1502.03167v3](https://arxiv.org/abs/1502.03167v3)
- Jain AK (2004) An introduction to biometric recognition. In: IEEE transactions on circuits and systems for video technology, pp 4–20
- Jain AK (2006) A tool for information Security. In: IEEE transactions on information forensics and security, pp 125–143
- LeCun Y, Bengio Y, Hinton G (2015) Deep learning. Nature 521(7553):436–444
- Liu Y, Li H, Wang X (2017) Rethinking feature discrimination and polymerization for large-scale recognition. arXiv preprint [arXiv:1710.00870](https://arxiv.org/abs/1710.00870)
- Liu N, Zhang M, Li H, Sun Z, Tan T (2016) Deepiris: learning pairwise filter bank for heterogeneous iris verification. Pattern Recognit Lett 82:154–161
- Mariana-Iuliana G, Radu T, Marius P (2019) Local learning with deep and handcrafted features for facial expression recognition. [arXiv:1804.10892v6](https://arxiv.org/abs/1804.10892v6)
- NIST (2012) IREX III—performance of iris identification algorithms. In: National Institute of Science and Technology, USA, Technical Report NIST Interagency Report 7836
- Omara I, Li F, Zhang H, Zuo W (2016) A novel geometric feature extraction method for ear recognition. Expert Syst Appl 65:127–135
- Patel V, Ratha N, Chellappa R (2015) Cancelable biometrics: a review. In: IEEE signal processing magazine, pp 54–65
- Pedro L, Galdamez P, Raveane W (2016) A brief review of the ear recognition process using deep neural networks. J. Appl. Logic 24:62–70
- Pei S, Chen M, Yu Y, Tang S, Zhong C (2017) Compact LBP and WLBP descriptor with magnitude and direction difference for face recognition. In: Proceedings of the IEEE international conference on image processing (ICIP), pp. 1067–1071
- Phillips P, Scruggs W, O'Toole A, Flynn P, Bowyer K, Schott C, Sharpe M (2010) Frvt 2006 and ice 2006 large scale experimental results. In: IEEE transactions on pattern analysis and machine intelligence, pp 831–846
- Pichao W, Zhaoyang L, Yonghong H, Wanqing L (2016) Combining convnets with hand-crafted features for action recognition based on an HMM-SVM Classifier. In: Proceedings of computer vision and pattern recognition (CVPR). [arXiv:1602.00749](https://arxiv.org/abs/1602.00749)
- Pillai JK, Patel VM, Chellappa R, Ratha N (2010) Sectored random projections for cancelable iris biometrics. In: IEEE international conference on acoustics speech and signal processing, pp 1838–1841
- Polash P, Gavrilova M, Klimenko S (2014) Situation awareness of cancelable biometric system. J Vis Comput 30:1059–1067
- Ratha N, Connell J, Bolle R, Chikkerur S (2006) Cancelable biometrics: a case study in fingerprints. In: International conference of pattern recognition, pp 370–373
- Ratha N, Chikkerur S, Connell J, Bolle R (2007) Generating cancelable fingerprint templates. IEEE Trans Pattern Anal Mach Intell 29:561–572
- Rathgeb C (2010) A secure iris recognition based on local intensity variations. In: Proceedings of the 7th international conference on image analysis and recognition, pp 266–275
- Rathgeb Ch, Barrero M, Busch Ch, Galbally J, Fierrez J (2015) Towards cancelable multi-biometrics based on bloom filters: a case study on feature level fusion of face and iris. In: 3<sup>rd</sup> International workshop on biometrics and forensics (IWBF)
- Rathgeb C, Breitinger F, Busch C, Baier H (2014) On the application of bloom filters to iris biometrics. IET J Biom 3(4):207–218
- Rathgeb C, Breitinger F, Baier H, Busch C (2015) Towards bloom filter-based indexing of iris biometric data. In: 15th IEEE international conference on biometrics, pp 422–429
- Sarbadhikari S, Basak J, Pal S, Kundu M (1998) Noisy fingerprints classification with directional based features using MLP. Neural Comput Appl 7:180–191
- Sh X, Jinhui T, Hanjiang L, Zhiheng N, Shuicheng Y (2016) Kinship Guided Age Progression. Pattern Recognit 59:156–157
- Sun Y, Wang X, Tang X (2015) Deeply learned face representations are sparse, selective, and robust. In: IEEE conference on computer vision and pattern recognition
- Swathi K, Kalyana V, Quek C (2018) Evolutionary based ICA with reference for EEGμRhythm Extraction. In: IEEE Access, pp 19702–19713
- Sylvia W, Kamalahardharini T (2017) Robust face recognition and classification system based on SIFT and DCP techniques in image processing. In: Proceedings of the international conference on intelligent computing and control (I2C2), pp 1–8
- Taigman Y, Yang M, Ranzato M, Wolf L (2014) Deepface: closing the gap to human-level performance in face verification. In: Proceedings of IEEE CVPR, pp 1701–1708
- Taigman Y, Yang M, Ranzato M, Wolf L (2015) Web-scale training for face identification. In: IEEE conference on computer vision and pattern recognition
- Sun Y, Liang D, Wang X, Tang X (2015) DeepID3: Face recognition with very deep neural networks. [arXiv:1502.00873](https://arxiv.org/abs/1502.00873)
- Tarek M, Ouda O, Hamza T (2017) Pre-image resistant cancelable biometrics scheme using bidirectional memory model. Int J Netw Secur 19(4):498–506
- Teoh ABJ, Ngo DCL, Goh A (2004) Biohashing: two factor authentication featuring fingerprint data and tokenised random number. Pattern Recognit 37(11):2245–2255
- Theodoridis S, Koutroumbas K (2008) Pattern recognition, 4th edn. Academic Press, Cambridge
- Tomas M, Sule Y, Jon Y (2016) Combining deep learning and hand-crafted features for skin lesion classification. In: Sixth international conference on image processing theory, tools and applications (IPTA)
- Vinay A, Kumar C, Shenoy R (2015) ORB-PCA based feature extraction technique for face recognition. In: Proceedings of the second international symposium on computer vision and the internet, pp 614–621
- Xiaolin X, Yicong Z (2019) Two-dimensional quaternion PCA and sparse PCA. IEEE Trans Neural Netw Learn Syst 30(7):1–15. <https://doi.org/10.1109/TNNLS.2018.2872541>
- Xu X, Lu L, Zhang X, Lu H, Deng W (2016) Multispectral palmprint recognition using multiclass projectionextreme learning machine and digital shearlet transform. Neural Comput Appl 27:143–153
- Yakopcic C, Alom M, Taha T (2017) Extremely parallel memristor crossbar architecture for convolutionalneural network implementation. In: Proceedings of the international joint conference on neural networks (IJCNN), pp 1696–1703
- Yang G, Shi D, Quek C (2005) Fingerprint minutia recognition with fuzzy neural network. In: Wang J, Liao X-F, Yi Z (eds) ISNN

- 2005, Part II. LNCS, vol 3497. Springer, Heidelberg, pp 165–170 (2005)
- Yong-Xia L, Jin Q, Rui X (2010) A new detection method of singular points of fingerprints based on neural network. In: The 3rd IEEE international conference on computer science and information technology, ICCSIT
- Yuan Z, Liu Y, Yue J, Li J, Yang H (2017) CORAL: coarse-grained reconfigurable architecture for convolutional neural networks. In: Proceedings of the IEEE/ACM international symposium on low power electronics and design (ISLPED), pp 1–6
- Zhang X, Ren S, Sun J (2016) Deep residual learning for image recognition. In: Proceedings of the IEEE conference on computer vision and pattern recognition, pp 770–778
- Zhao H, Sun M, Deng W, Yang X (2017) A new feature extraction method based on EEMD and multi-scale fuzzy entropy for motor bearing. Entropy 19:14
- Zhao H, Yao R, Xu L, Yuan Y, Li G, Deng W (2018) Study on a novel fault damage degree identification method using high-order differential mathematical morphology gradient spectrum entropy. Entropy 20:682
- Zheng Y, Pal D, Savvides M (2018) Ring loss: convex feature normalization for face recognition. In: CVPR
- Zhu E, Yin J, Hu C, Zhang G (2005) Quality estimation of fingerprint image based on neural network. In: Wang L, Chen KS, Ong Y (eds.) ICNC 2005, Part II. LNCS, vol. 3611, pp. 65–70. Springer, Heidelberg
- Zuo J, Ratha NK, Connell JH (2008) Cancelable iris biometric. In: Proceedings of the 19th international conference on pattern recognition, pp 1–4

**Publisher's Note** Springer Nature remains neutral with regard to jurisdictional claims in published maps and institutional affiliations.

## Affiliations

**Essam Abdellatef<sup>1</sup> · Eman M. Omran<sup>2</sup> · Randa F. Soliman<sup>3</sup> · Nabil A. Ismail<sup>4</sup> · Salah Eldin S. E. Abd Elrahman<sup>4</sup> · Khalid N. Ismail<sup>5,6</sup> · Mohamed Rihan<sup>7</sup> · Fathi E. Abd El-Samie<sup>7,8</sup> · Ayman A. Eisa<sup>2</sup>**

<sup>1</sup> Electronics and Communication Department, Delta Higher Institute for Engineering and Technology (DHET), Mansoura, Egypt

<sup>2</sup> Department of Nuclear Safety and Radiological Emergencies, NCRRT, Egyptian Atomic Energy Authority (EAEA), Cairo, Egypt

<sup>3</sup> Mathematics and Computer Science Department, Faculty of Science, Menoufia University, Menouf Governorate 32511, Egypt

<sup>4</sup> Department of Computer Science and Engineering, Faculty of Electronic Engineering, Menoufia University, Menouf 32952, Egypt

<sup>5</sup> Department of Computer Science, Durham University, Durham DH1 3LE, UK

<sup>6</sup> Information Technology Department, Faculty of Computers and Information, Menoufia University, Al Minufiyah, Egypt

<sup>7</sup> Department of Electronics and Electrical Communications Engineering, Faculty of Electronic Engineering, Menoufia University, Menouf 32952, Egypt

<sup>8</sup> Department of Information Technology, College of Computer and Information sciences, Princess Nourah Bint Abdulrahman University, Riyadh, Saudi Arabia